International Journal of Mechanical, Industrial and Aerospace Sciences
ISSN: 2517-9950
Vol:6, No:8, 2012

A Study on the Effect of Variation of the Cross-sectional Area of Spiral Volute Casing for Centrifugal Pump

Hyun Bae Jin, Myung Jin Kim, Wui Jun Chung

***Abstract*—**The impeller and the casing are the key components of a centrifugal pump. Although there have been many studies on the impeller and the volute casing of centrifugal pump, further study of the volute casing to improve the performance of centrifugal pumps is needed. In this paper, the effect of cross-sectional area on the performance of volute casing was investigated using a commercial CFD code. The performance characteristics, not only at the off-design point but also for a full type model are required these days. So we conducted numerical analysis for all operating points by using complete geometry through transient analysis. Transient analysis on the complete geometry of a real product has the advantage of simulating realistic flow. The results of this study show the variation of a performance curve by modifying the above-mentioned design parameter.

***Keywords*—**Centrifugal Pump, Volute Casing, Cross-Section area, CFD

I. Introduction

A centrifugal pump which is widely used throughout industry is a typical turbo-machinery that converts external mechanical energy into pressure and kinetic energy of fluid. It consists of an impeller and volute casing. An impeller is a mechanical device that supplies mechanical energy to fluid and is a key component of any centrifugal pump.

Therefore, up to now, many studies have focused intensively on impellers. Fluid that obtains energy from an impeller is discharged through a volute casing, so the characteristics of the volute casing are an important factor if the goal is to discharge fluid with less energy loss. Thus study on the characteristics of the volute casing is absolutely a necessary process to improve the performance of centrifugal pumps. But most studies have focused on the impeller while study of the volute casing has drawn relatively little attention, but in order to improve the performance of centrifugal pumps, a more sophisticated study of volute casing is needed.

Yang and Kong investigated the effect of volute throat area on the efficiency curve of centrifugal pumps [1]. In the case of the increase of volute throat area, the results show that pump BEP moves to the high flow region and slightly decreases, and the performance curve becomes flatter.

Hyun Bae Jin is with the Mechanical Engineering Department, University of Ulsan, Ulsan, Republic of Korea (phone: 82-052-259-1614; e-mail: puhahazzang7@ mail.ulsan.ac.kr).

Myung Jin Kim is with the Mechanical Engineering Department, University of Ulsan, Ulsan, Republic of Korea (phone: 82-052-259-1614; e-mail: korykmj@ mail.ulsan.ac.kr).

*Wui Jun Chung is with the Mechanical Engineering Department, University of Ulsan, Ulsan, Republic of Korea (e-mail: wjchung@ mail.ulsan.ac.kr)

Chan and Wong compared two different design techniques that have been conventionally used in the design of the volute for centrifugal pumps [2], and investigated the effects of the position of the tongue and effects of the radial gap between the impeller and the volute casing of the centrifugal blood pump with ultra-low specific speed [3].

In this study, to understand characteristics of the volute casing of centrifugal pumps, we investigated the effects of a design parameter of the volute casing on the performance of a centrifugal pump by using commercial CFD code. The selected parameter was cross-sectional area size. The reason that this parameter was selected was to improve performance without any large modification of the product.

II. Numerical Analysis

A. Model and Grid

The centrifugal pump selected for analysis is a typical single stage volute pump used in industry. It has a rotational speed of 1750rpm, flow 66 m^3/h, head 32m on-design point, and 6 blades. Analysis was conducted on the complete geometry of the full model with the volute casing to obtain more accurate results in a realistic flow. In other words, complicated and various flows were formed in the 6 impeller passages because of the asymmetry of volute casing. So the full model geometry is necessary for the analysis. The geometry of the used pump was obtained by 3D scanning. The impeller geometry used for analysis was revised by ANSYS Blade Editor; the coordinate data of the impeller can be obtained on the ANSYS Blade Editor by defining the meridian. The grids used in this study were made with ANSYS Turbo-Grid for the impeller and with ANSYS ICEM CFD for the volute casing. The geometry and the grid used for this analysis are shown in Fig. 1.

To obtain precise results from numerical analysis, not only the number of grids but also y+ are important. In this study, in which the SST turbulence model was used, the value of y+ was selected to be less than 1.

The number of grids was selected via the comparison of experimental data through trial and error; the number of grids was about 200,000 per blade on the impeller and 2,500,000 on the volute, so the total was about 3,700,000.

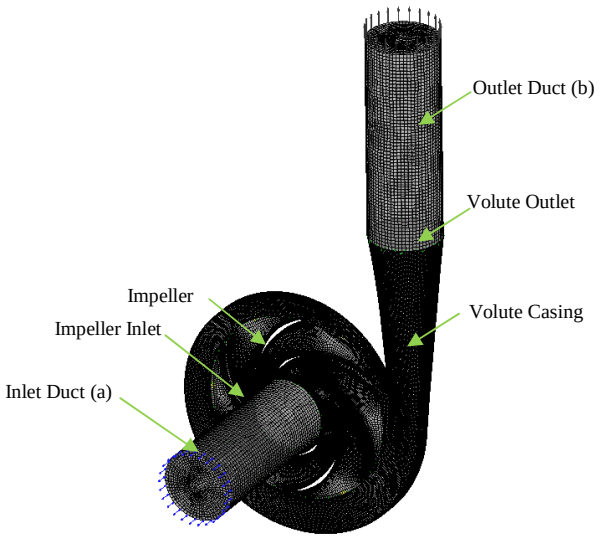

Fig. 1 Geometry of centrifugal pump and grid

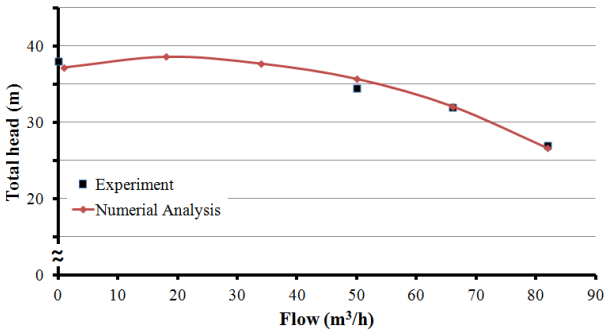

Fig. 2 Comparison between the performance curves of experimental and numerical analysis

TABLE I
TOTAL HEAD COMPARISON FOR EXP. AND NUMERICAL ANALYSIS

Flow (m^3/h)	0	18	34	50	66	82
Exp.(m)	37.4	-	-	34.5	32.0	27.0
Num.(m)	37.2	38.6	37.7	35.7	32.1	26.6
Error(%)	2.11	-	-	3.48	0.31	1.48

The numerical analysis results compared with experimental data are shown in Fig. 2 and Table I. As shown in Table I, our selection of the number of grids is reasonable because the error between experimental data and numerical analysis data is less than 4%.

To investigate the performance curve according to variation of the volute casing cross-sectional area, five casing models were investigated. The original standard shape of the volute casing which uses the principle of the Archimedes spiral that was proposed by Stepanoff [4] and other 4 models were designed. Fig. 3 and Table II show the position of the volute casing cross-section and area for five models. In Fig. 3, section 8 is the throat and the position of the tongue is 25° from section 8.

Fig. 4 represents the five cases (-30%, -10%, standard, +10%, +30%) of the cross-sectional area based on the standard model.

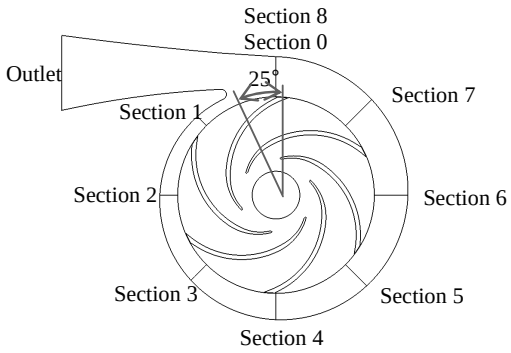

Fig. 3 The position of the sections

TABLE II
VARIATION OF VOLUTE CROSS-SECTION AREA

Model	-30%	-10%	Stand	+10%	+30%
Section 2 ($\times 10^{-3} m^2$)	0.25609	0.32925	0.36584	0.40242	0.47556
Section 4 ($\times 10^{-3} m^2$)	0.51217	0.65851	0.73167	0.80484	0.95118
Section 6 ($\times 10^{-3} m^2$)	0.76826	0.98776	1.09751	1.20726	1.42676
Section 8 ($\times 10^{-3} m^2$)	1.02434	1.31701	1.46334	1.60968	1.90235

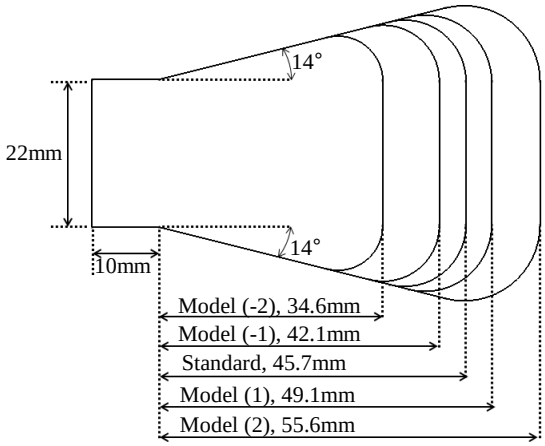

Fig. 4 The shape of the cross-sectional area of section 8

B. Method

ANSYS CFX 13, a commercial CFD code, was used to conduct numerical analysis. Boundary conditions were total pressure at inlet and six flows of $0\,m^3/h$, $18\,m^3/h$, $34\,m^3/h$, $50\,m^3/h$, $66\,m^3/h$, and $82\,m^3/h$ at outlet. To minimize the effect of the boundary conditions, constant area ducts that are three-times of the pipe in diameter were installed at the inlet and outlet as shown in Fig.1 (a) and (b). Although these ducts were installed, the measured position of pressure and velocity to express performance curves were impeller inlet and volute outlet. This is because total head is defined as the energy differential between impeller inlet and volute outlet [4].

TABLE III
CALCULATION CONDITIONS

Working Fluid	Water
Turbulence Model	SST model
Boundary condition	Inlet: Total Pressure Outlet: Mass flow
Interface	Transient Rotor Staor
Time step	2.857×10^{-4}s
Total time	0.3425s

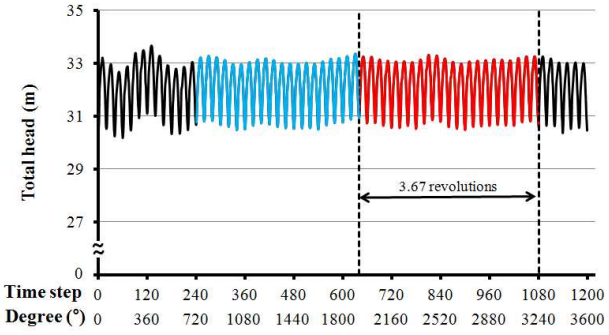

Fig. 5 The solution of transient analysis

The working fluid was water. The turbulence model is Shear Stress Transport (SST) which can accurately analyze wall shear flow such as separation. The Transient Rotor Stator model was applied at the interface between rotation and stationary. The time step and total time used in this analysis were 2.857×10^{-4}s and 0.3425s, respectively, and they mean the time for 3 degrees of rotation of the impeller and 10 impeller revolutions, respectively. To quickly converge, the output of the steady analysis was used as the initial condition. Fig. 6 shows the variation of the head for 10 revolutions. As shown in Fig. 5, as a result of all the tests, when the impeller rotates more than approximately 7 revolutions, the pattern of solution becomes stable with specific periodicity. So, we obtained the solution of the transient analysis by averaging approximately 3 revolutions (the red color of Fig.5).

III. RESULT AND DISCUSSION

The performance curve of a typical centrifugal pump shows a rightward rising curve from the cut-off point as in Fig. 2. This is the curve in which loss by collision, friction, and slip is subtracted from the ideal head curve. In pipe systems including the centrifugal pump with the above-mentioned performance curve, when an energy storage device is installed in the middle of the discharge pipe, the possibility that a surge occurs in the pipe system increases. So the shape of the performance curve of a centrifugal pump is very important.

Therefore the effect of the variation of cross-sectional area was investigated as a simple way to improve the stability of pipe systems, including the centrifugal pump in this study. The results here are the averaged value of the transient analysis result that has the periodicity of the stabilized specific pattern mentioned in Fig. 5.

Fig. 6 shows the static pressure coefficient at the volute casing inlet of the circumferential direction from the tongue to the outlet via the throat in a volute casing in which the trailing edge of the impeller is positioned at 4 points such as 25°(0°), 40°(15°), 55°(30°), and 70°(45°), while the impeller rotates at design flow.

While the impeller rotates one pitch (60°), the figure on the upper part of Fig. 6 represents the total head at the volute outlet and the four points here are measured at the same time (angle) with four color lines of static pressure head coefficient curves. The averaged value of the four points is only one value on the outlet cross-sectional area of the volute casing. The measured points are on the mid-span of the shroud and hub because this plane can be representative of a flow field.

Most of the graphs are presented as velocity coefficients and head coefficients as in the following equations.

$$\varphi = \frac{v_R}{u_2} \text{ or } \frac{v_C}{u_2}$$

$$\psi = \frac{g \cdot H}{u_2^2}$$

v_R, v_C, u_2, g and H stand of radial velocity, circumferential velocity, peripheral velocity, gravitational acceleration and energy head, respectively.

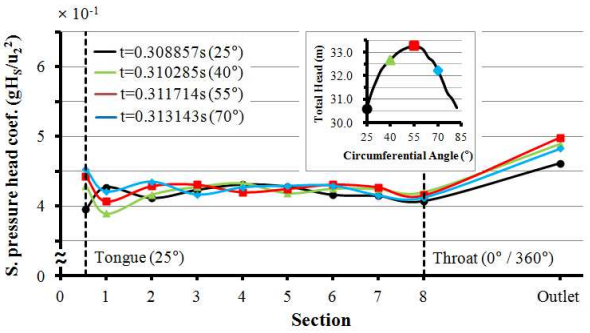

Fig. 6 Static pressure coefficients according to circumferential direction at the volute casing inlet at design flow of the standard model

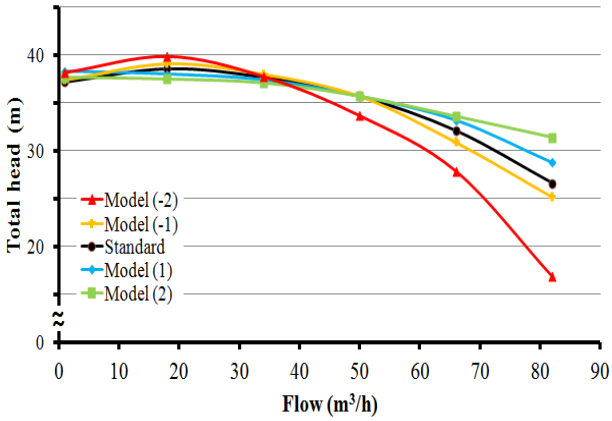

Fig. 7 Total head curves according to flow

TABLE IV
THE TOTAL HEAD DIFFERENCE FOR 4 MODELS

Flow (m^3/h)	0	18	34	50	66	82
Model (-2) (%)	2.69	3.37	0.27	-5.60	-13.1	-36.5
Model (-1) (%)	0.54	1.30	0.80	0	-3.74	-5.26
Stand.	Basis	Basis	Basis	Basis	Basis	Basis
Model (1) (%)	2.96	-1.55	-0.80	0	3.43	8.27
Model (2) (%)	1.34	-2.85	-1.59	0	4.67	18.05

To analyze the effect of variation of the cross-sectional area, numerical analysis was performed for five different models and the result is presented in Fig. 7 and Table IV. The standard model is the basic volute casing in use currently. Model (1) and model (-1) are only 10% larger and 10% smaller than the standard cross-sectional area. Model (2) and Model (-2) are also 30% larger and 30% smaller, respectively.

In the case of the larger models like Model (1) and Model (2), the performance curves show a flat tendency overall because the curves, according to variation of the cross-sectional area, decrease from the cut-off point rightward. But in the case of the smaller models like Model (-1) and Model (-2), the curves show an increase and decrease rightward, when compared to the standard model, the from cut-off point. Especially, Model (-2), which is the smallest model, shows this tendency most obviously. As mentioned earlier, in the case of a rightward increasing and decreasing curve, there is the possibility that a surge may occur. Therefore, one important benefit of having a larger cross-sectional area is that this is a good way of preventing surges.

The curves of the four models, except Model (-2), show the same value at flow 50 m^3/h, and the order change of the curve is shown from this flow. In other words, the curves show a lower value at low flow and a higher one at high flow with lager cross-sectional area. On the other hand, Model (-2) shows the regular order value with the other four models at low flow. But the tendency is away from regular variation and an abrupt decrease of the head is shown at high flow. Then, the position of the same value with the standard model shifts to the lower flow and the shape of the curve becomes a rising and falling curve rightward. Finally such a model becomes a sensitive curve to surges. To investigate this phenomenon for the effect of the cross-sectional area, numerical analysis was performed for Model (-2), the standard model, and Model (2) at low, design and high flow.

To investigate the effect of periodicity, the variation of velocity vector by rotation of the impeller is presented in Fig. 8 and Fig. 9 according to variation of flow. In these figures, 25°(t=0.308857s) means when the tongue and a blade meet, while 55°(t=0.311714s) means when the tongue is positioned in the middle of a pitch of the impeller. In these figures, the periodic phenomenon occurs obviously because the flow is different according to the position of the impeller regardless of flow and model. Also backward flow occurs at the impeller outlet in the circumferential direction regardless of the position of the impeller at low flow in the standard model or others.

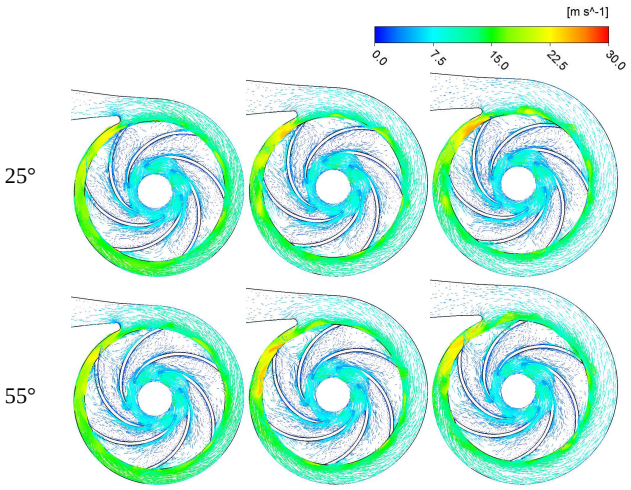

(a) Model (-2) (b) Standard (c) Model (2)

Fig. 8 Velocity vector according to model for 18 m^3/h at z/b_2 = 0.5

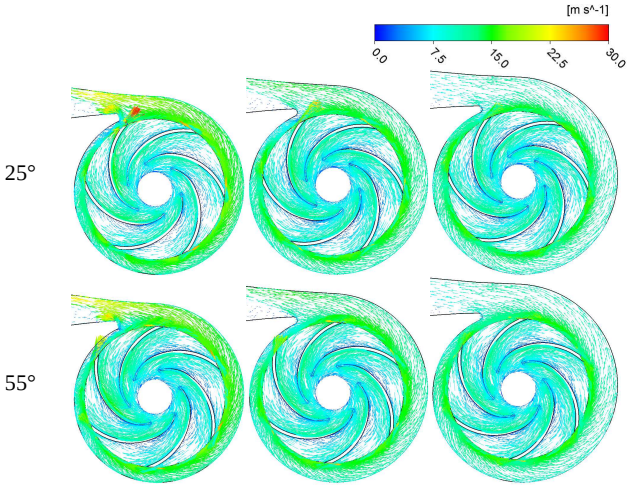

(a) Model (-2) (b) Standard (c) Model (2)

Fig. 9 Velocity vector according to model for 82 m^3/h at z/b_2 = 0.5

The backward flow shown in Fig. 8 and Fig. 9 results in circulation in the impeller and energy loss occurs because of this. To investigate this backward flow, the radial velocity of the standard model at the volute casing inlet by the rotation of the impeller is presented in Fig. 10. In this figure, the x-axis and y-axis refer to circumferential position and radial velocity, respectively, and the dashed lines at 25° and 360° indicate the tongue and the throat of the volute casing. A negative value indicates backward flow into the impeller.

In Fig. 10(b), the radial velocity component near the volute tongue became slightly larger toward both the negative and positive directions at design flow. But there was no the backward flow velocity overall and the forward flow velocity component only repeated regularly. Operation of the standard model at design flow was significantly stable because of the uniform radial velocity.

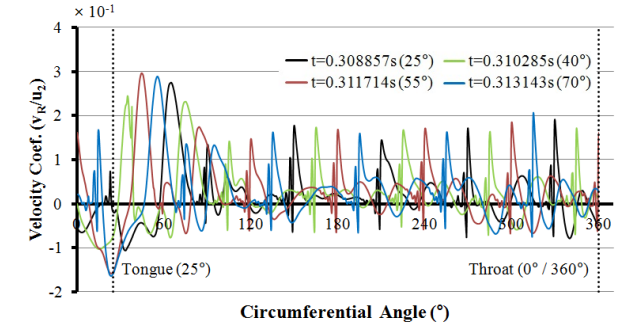

(a) 18 m^3/h

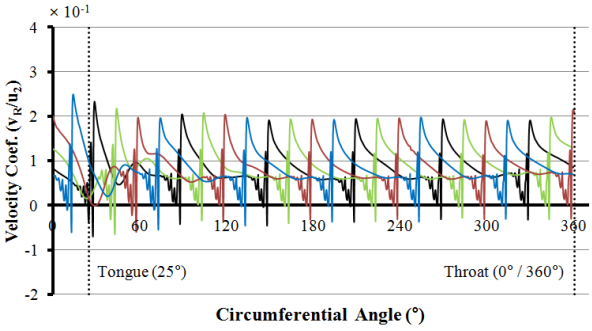

(b) 66 m^3/h

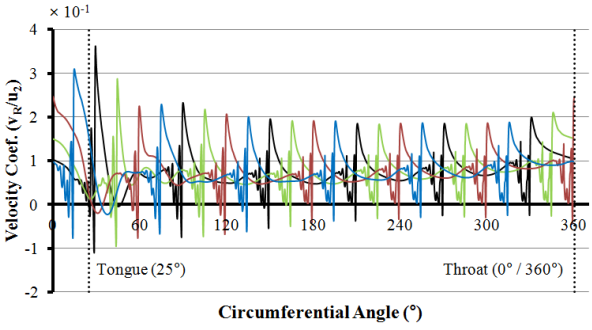

(c) 82 m^3/h

Fig. 10 Radial velocity according to circumferential angle at volute casing inlet and z/b_2 =0.5 on the standard model

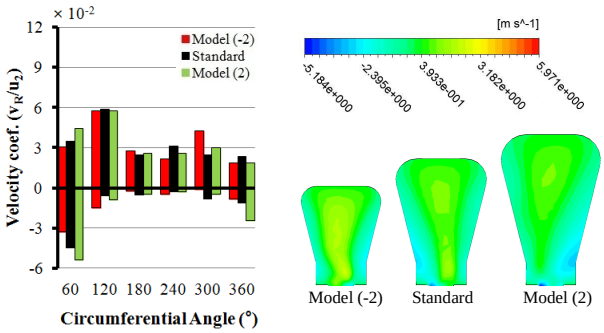

(a) 18 m^3/h

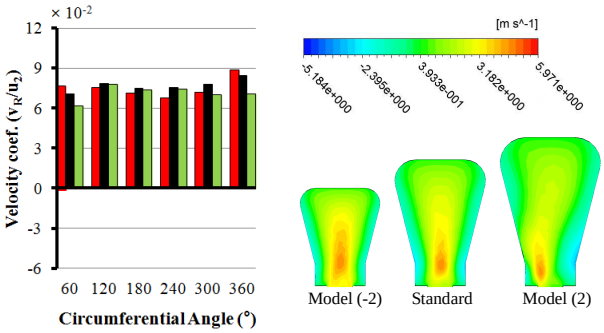

(b) 66 m^3/h

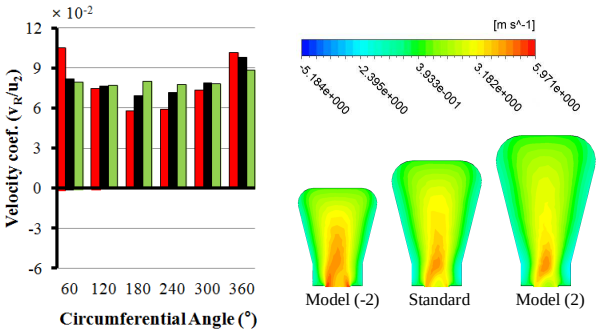

(c) 82 m^3/h

Fig. 11 Average radial velocity according to circumferential angle at volute casing inlet and z/ b_2 = 0.5 and radial velocity distribution according to model at section 8

In Fig. 10(a), the backward flow is shown throughout the entire region and it is distributed especially widely between the tongue and throat in low flow. A large forward flow is shown from near the tongue to about 90°. This is the reason why sufficient space is generated because of a small amount of discharging flow against the large space between the tongue and throat and so a large backward flow occurs. As a result, the large accumulated flow in the impeller receives a large centrifugal force and this flow is discharged simultaneously when the impeller passes through the tongue.

In Fig. 10(c), the flow pattern is similar to that of the design flow except that the forward flow near the tongue and so the standard model in high flow is more stable than in low flow. As high flow contributed significantly to forward flow velocity this is a reasonable result.

To investigate the tendency of radial velocity distribution according to the size of volute casing cross section, the result of the forward and backward flow for Model (-2), the standard model, and Model (2) are presented in the left figure of Fig. 11. Here the x-axis refers to the regions divided into segments of 60° in the circumferential direction. In addition, radial velocity with a positive value results in friction and collision with walls and affects vortex and static pressure. Also, to investigate the tendency of the final radial velocity within the volute casing, the radial velocity distribution of section 8 (throat) is presented in the right figure of Fig. 11.

The three colors indicate Models (-2), the standard model, and Model (2), respectively.

In Fig. 11(a) shows that with low flow, backward flow occurs overall and forward and backward flow are nearly equal to each other from the throat to about 60°. Backward flow and accumulation around this region and a large discharge after passing through the tongue have already been mentioned. After that, the discharging force decreases and backward flow becomes weak because of the initial large outflow. In addition backward flow reoccurs around the throat. In Fig. 11(b) as design flow, there was little backflow into the impeller. Also, the standard model in this figure shows uniform flow along the circumferential direction. In Fig. 11(c), in the case of high flow, backward flow also does not occur as at design flow. The forward flow becomes nearly uniform with increasing cross-sectional area. This shows that stable operation is possible with increasing the cross-sectional area at high flow. On the other hand, the forward flow does not become uniform with decreasing cross-sectional area. In other words, this operation is unstable because the forward flow occurs strongly around the tongue and the throat but occurs weakly around 180°~240°.

Radial velocity into the volute casing results in vortex, friction, and collision and the remaining rest energy is converted into static pressure. So the radial velocity distribution is a very important factor in the study of the performance curve. The right figure of Fig. 11 shows the radial velocity distribution at section 8 (throat). In this figure, similar distributions are shown at low flow rate regardless of model and the effects for model and flow are ambiguous and the similar flow patterns are shown at high flow. Though there is a little difference in the various flows, the strong radial velocity is shown in the center of the volute casing for all models and flows. Loss and total head are affected by vortex and static pressure in the internal flow of the volute casing. So the vortex distribution and the static pressure distribution at section 8 are presented in Fig. 12.

In Fig. 12 (b), as the design flow, the vortex shape of the standard model has a slightly asymmetric structure, Model (-2) is more symmetric than the standard model, and Model (2) doesn't have a symmetric structure. In other words, the shape of the vortex becomes symmetric with increasing cross-sectional area. Van den Braembussche [5] claims that ideal flow is when two vortices occur symmetrically in the volute casing. Therefore the most ideal shape of vortex in the above model is the vortex of Model (-2). But Model (-2) with the most asymmetric structure is the highest and Model (2) with the most symmetric structure is the lowest for static pressure. Strong radial velocity occurs at the center of the area because the design flow is excessive quantity to Model (-2), which is smaller than the standard model in the cross-sectional area. So low static pressure is distributed. On the other hand, static pressure in Model (2) becomes high for the opposite reason.

In Fig. 12 (a), which shows low flow, the very weak radial velocity and the asymmetric shape of vortex occur because of lower flow than at design flow. Also, the static pressure is barely affected by the variation of model.

In Fig. 12 (c), which shows high flow, the structure of vortex presents obvious symmetry regardless of the model, unlike at design flow because of higher flow than at design flow.

This fact can be confirmed obviously in Model (2). Radial velocity is slowed down because of the increase of the cross-sectional area and the tendency of static pressure is similar to at design flow.

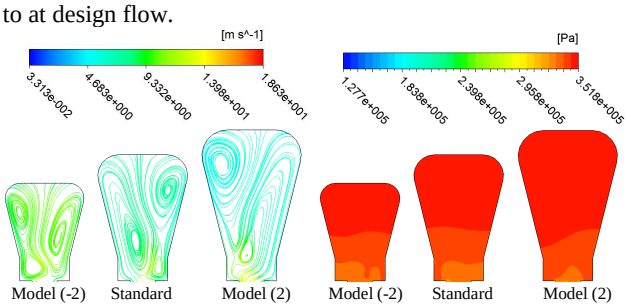

(a) 18 m^3/h

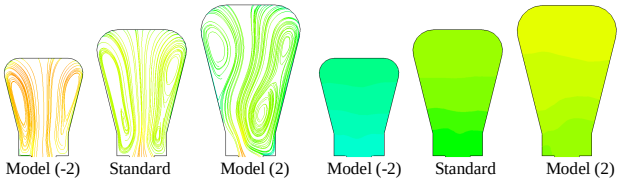

(b) 66 m^3/h

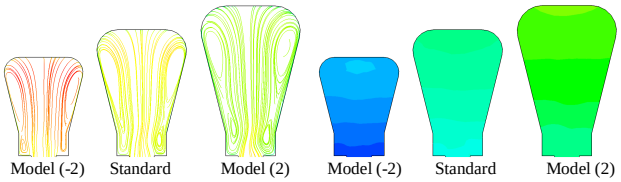

(c) 82 m^3/h

Fig. 12 Vortex and static pressure distribution according to model at section 8

So the ideal flow appears when the flow is higher and cross-sectional area is smaller. Therefore the symmetry of vortex is affected by the flow against the area. The cross-sectional area is not an important factor on the static pressure development at low flow but cross section area affects static pressure development when the flow is larger than the design flow.

The performance curve also is affected by velocity head. Therefore the analysis for circumferential velocity in the volute casing is important. To investigate the general tendency, the circumferential velocity distribution at the volute casing inlet along the impeller rotation angle is presented in Fig. 13. The four colors have the same meaning as in Fig. 10.

Fig. 13(b) shows that at design flow velocity immediately drops when the trailing edge of the impeller and the tongue meet but velocity distribution is uniform overall. Fig. 13(a) shows that in the case of a low flow velocity accelerates sharply when the trailing edge and the tongue meet.

But after passing through the tongue velocity drops. This phenomenon also is caused by backward flow from the throat to the tongue at low flow. The flow maintains averaged velocity from 120° but the flow is unstable because of irregular flow pattern.

In contrast, Figure 13 (c) shows that in the case of high flow velocities slow down when the trailing edge and the tongue meet. This phenomenon is the reason why flow passage is blocked temporarily because of strong radial velocity and collision near the tongue.

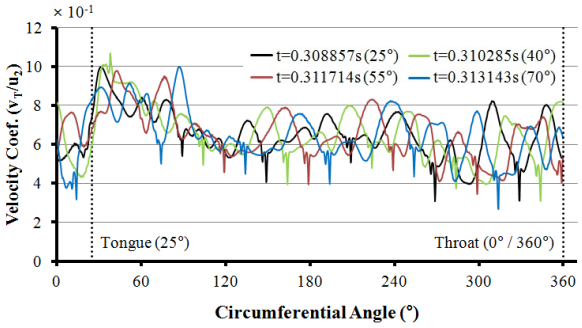

(a) 18 m^3/h

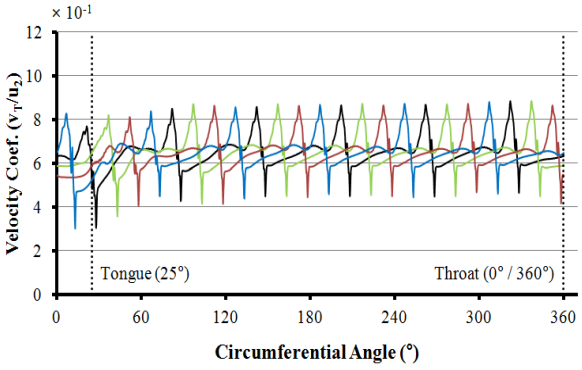

(b) 66 m^3/h

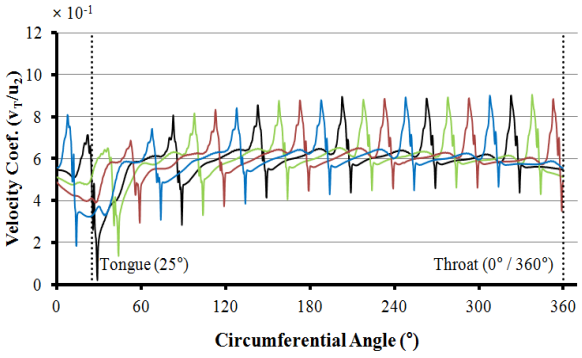

(b) 82 m^3/h

Fig. 13 Circumferential velocity according to circumferential angle at volute casing inlet and z/b_2 = 0.5 in the standard model

To investigate the effect of circumferential velocity at each section of circumferential direction, the average value of circumferential velocities at the cross sectional area of the interval of 60° is presented in left figure of Fig. 14. The dynamic pressure distributions that developed at section 8 (throat) are also presented in the right figure of Fig. 14.

Three colors indicate Model (-2), the standard model, and Model (2) respectively.

In Fig. 14(b) with the design flow, as mentioned above, passing through the tongue, the velocity of Model (-2) becomes high from low, Model (2) becomes low from high because of high flow, and the standard model shows almost uniform velocity throughout the entire region. In the case of high flow, Model (2) keeps nearly uniform velocity because of sufficient space while other models show a tendency to increase with different gradients. In the case of low flow, there are different decreases according to the model.

The velocities decrease from high velocity because of the accumulation of backward flow around the tongue, and this phenomenon is opposite to high flow.

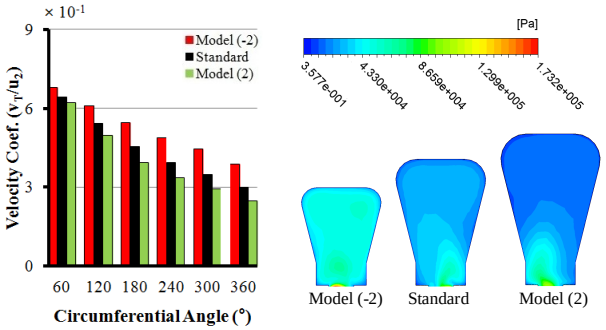

(a) 18 m^3/h

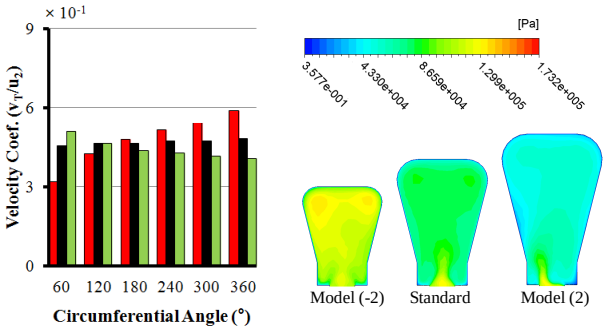

(b) 66 m^3/h

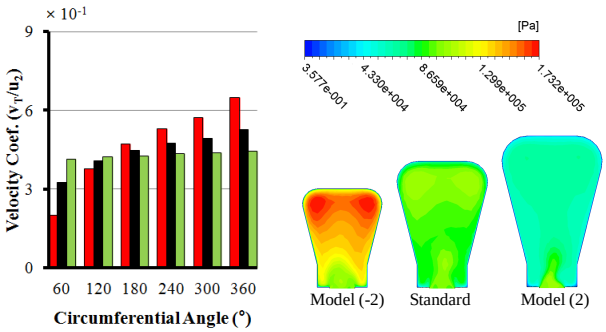

(c) 82 m^3/h

Fig. 14 Average circumferential velocity according to circumferential angle at volute casing inlet and z/ b_2 = 0.5 with dynamic pressure distribution according to model at section 8

In right figure of Fig. 14, it can be seen that the dynamic pressure increases with smaller cross-sectional area and higher flow.

The high dynamic pressure is developed at the inlet of the volute casing at low flow but the high dynamic pressure is developed farther away from the inlet at high flow. The dynamic pressure is nearly uniform throughout the entire region at design flow.

To investigate the effect of the static and dynamic pressure of the volute casing on the performance curve according to variation of flow, static pressure, dynamic pressure, and total pressure at each section in circumferential direction of the volute and discharge diffuser are presented in Fig. 15, Fig. 16, and Fig. 17.

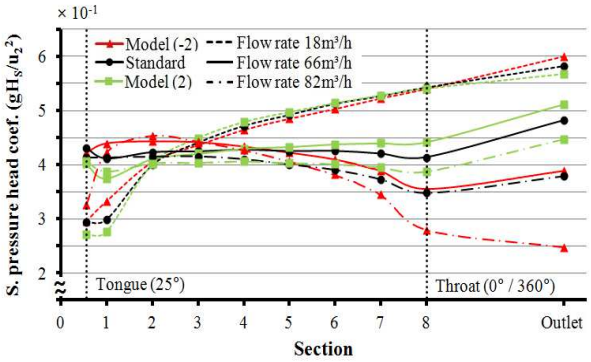

Fig. 15 Static pressure head according to circumferential section

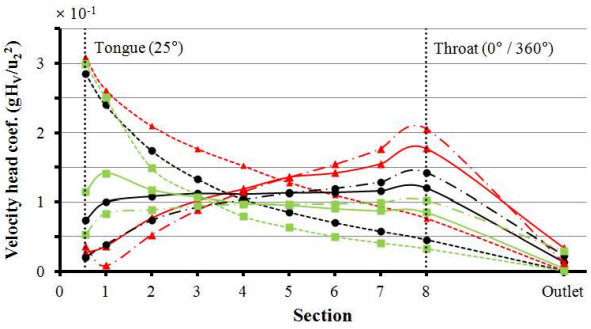

Fig. 16 Velocity head coefficient according to circumferential section

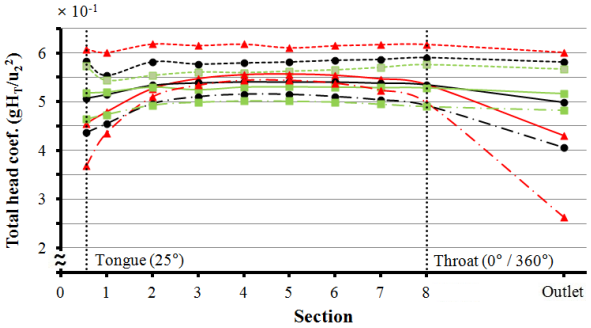

Fig. 17 Total head coefficient according to circumferential section

Fig. 15 presents the static pressure head coefficient. At design flow, Model (-2), the standard model, and Model (2) intersect at section 4 and the coefficient decreases, is uniform, and increases respectively from this section.

Model (-2) and Model (2) show the opposite tendencies. Static pressure head coefficients increase at the discharge diffuser. The recovery amounts are that Model (-2) is 0.033, the standard model is 0.069, and Model (2) is 0.07. In the case of larger one than the standard model, the recovery amount of Model (2) is about twice that of Model (-2).

At low flow, the static pressure head coefficient of the three models increases along the circumferential direction. The orders of the coefficients change because these curves intersect two times at section 2 and section 8. But there is little difference of the coefficients in the volute casing and discharge diffuser.

The recovery amounts are that Model (-2) is 0.059, the standard model is 0.039, and Model (2) is 0.027. The recovery amount of Model (-2) is about twice that of Model (2).

At high flow, the three models intersect near section 5 and show a similar tendency to design flow, but the coefficients slightly decrease after section 4. The standard model and Model (2) recovered as 0.030 and 0.060, respectively, in the discharge diffuser. On the other hand, because Model (-2) shows a unique phenomenon in that the coefficients do not recover so Model (-2) is not suitable at high flow. The coefficient curves of all models intersect each other at section 2 ~ section 4.

Fig. 16 shows the velocity head coefficients. In this figure, the three models intersect at section 4 as the tendency of static pressure head coefficients at design flow. The coefficient increases, is uniform, and decreases at Model (-2), the standard model, and model (2), respectively. The two models aside from the standard model are opposite in the tendencies of the coefficients. The coefficients decrease toward a similar value in section 8 ~ Outlet and the decreasing amounts are that Model (-2) is 0.143, the standard model is 0.107, and Model (2) is 0.081.

At low flow, all the three models decrease and show higher velocity head coefficients with smaller cross-sectional area and the tendency is opposite to the static pressure head coefficients at section 2 ~ section 8. The velocity head gathers at similar values in section 8 ~ Outlet as in the other models. The decreasing amounts are that Model (-2) is 0.079, the standard model is 0.045, and Model (2) is 0.032.

At high flow, the three models intersect at section 3 ~ section 4 and the coefficients increases with a similar tendency to design flow. The coefficients also are gathered at similar values in section 8 ~ Outlet and the decreasing amounts are that Model (-2) is 0.193, the standard model is 0.120, and Model (2) is 0.073.

Fig 17 shows total head coefficients. Total heads are nearly uniform for all models of each flow in section 2 ~ section 8 and the orders of the coefficients are in the reverse order of cross-sectional area like Model (-2), the standard model, and Model (2). There is a smaller difference of total head coefficients at design flow or higher and there is a larger difference of total head coefficients at low flow. At design and high flow, total head coefficients increase in section 1 ~ section 2, which are affected by the tongue, and intersect at section 2 and section 3, respectively.

However total head coefficients decrease and increase near the tongue and then are maintained uniformly without intersection at low flow. In the case of low flow, the order of the total head coefficients are maintained in the discharge diffuser as in the volute casing, but the total head coefficients decrease slightly. The decreasing amounts of the total head coefficients are that Model (-2) is 0.02, the standard model is 0.006, and Model (2) is 0.005. In contrast, at the design flow or larger, the total head coefficients curve intersects in section 8 again and the order of the total head coefficients is the same as the order of section 1 ~ section 2. Then the total head coefficients decrease in section 8 ~ Outlet and the decreasing amounts are the largest at high flow.

The decreasing amounts are that Model (-2) is 0.105, the standard model is 0.037, and Model (2) is 0.011 at design flow and is that Model (-2) is 0.235, the standard model is 0.086, and Model (2) is 0.008 at high flow.

Total head coefficients become almost constant at all flows and models. This is the reason that static pressure head coefficients increase and velocity head coefficients decrease at low flow and the opposite phenomena occur at high flow and total head coefficients, by summation of static pressure head coefficients and velocity head coefficients, are maintained nearly constant as at design flow.

In the discharge diffuser, the total head coefficients are almost uniform regardless of model at low flow but the decreasing amount grows larger along with increasing flow and smaller cross-sectional area.

The order of total head coefficients according to model at low flow are in the reverse order of that of design flow or larger. Also differences of static pressure head coefficients according to model are larger with higher flow and the tendency of the velocity head coefficients are opposite to that of the static pressure head coefficients.

Therefore when the centrifugal pump is operated at too high flow against cross-sectional area, the velocity head coefficient is not converted into static pressure head coefficient in section 8 ~ Outlet. So when a volute casing is designed, the above matter should be considered.

To investigate the characteristics of the performance curves of Fig. 7, total head curve coefficients for the five models at the flows of 18 m^3/h, 50 m^3/h, and 82 m^3/h are presented in Fig. 18, Fig. 19, and Fig. 20.

Fig. 18 shows the total head coefficients according to models at 18 m^3/h. The curves are uniform and higher with smaller cross-sectional area along circumferential direction in the volute casing and Model (-2) slightly decreases in section 8 ~ Outlet but the order of the curves is maintained to be that of the volute casing.

Fig. 19 shows the total head coefficients according to models at 50 m^3/h. Other models, except Model (-2), are almost uniform along circumferential direction regardless of cross-sectional area and show the same value at the volute outlet. But the value of Model (-2) increases slightly more than that of the other models in the volute casing and decreases relatively greatly in the discharge diffuser.

Fig. 20 shows total head coefficients at 82 m^3/h and the tendency is enlarged in the changing figures of the curves from 18 m^3/h to 50 m^3/h and the decreasing amounts are different according to model in the discharge diffuser.

In summary, total head decrease according to increasing flow regardless of model and decrease greatly with higher flow and smaller cross-sectional area. Therefore the effects on total head coefficients according to model are insignificant but larger loss occurs with smaller cross-sectional area at low flow and total head coefficients decrease significantly at high flow. As a result, the total head coefficient curve with a possibility of a surge occurring is made at high flow.

As mentioned above, the discharge diffuser at section 8 ~ Outlet is the device that maximizes the static pressure energy in the fluid energy obtained from the centrifugal pump, so this plays a very important role in determining the performance curve. Table V presents the recovery amount of each curve and the ratio of total head recovery to static pressure head recovery for the models and flows.

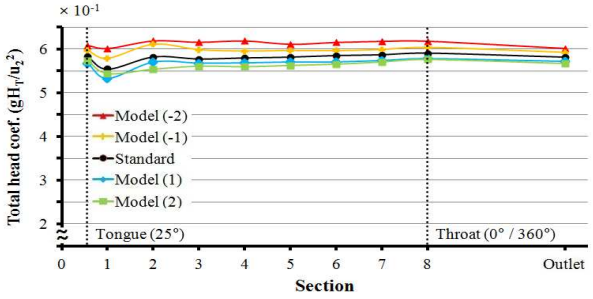

Fig. 18 Total head coefficients of models according to circumferential section at 18 m^3/h

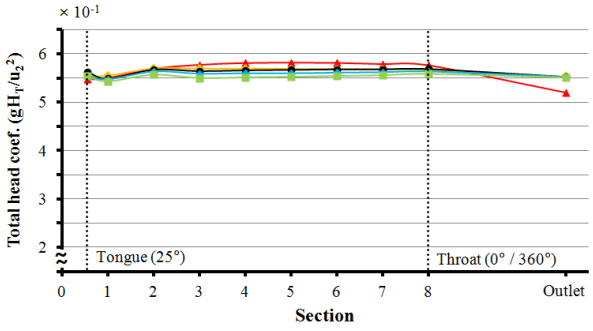

Fig. 19 Total head coefficient of models according to circumferential section at 50 m^3/h

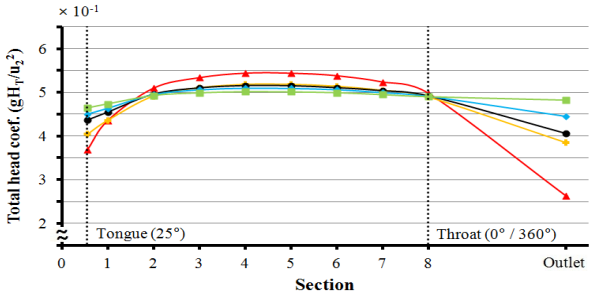

Fig. 20 Total head coefficient of models according to circumferential section at 82 m^3/h

This ratio means the decreasing amount of total head against the variation amount of static pressure head and the loss is lower with lower figures in the decreasing amount of total head. So, above table can be important parameter to select model for variation of flow. In this table, Model (1) is most reasonable at $18\,m^3/h$ and Model (2) is reasonable at $50\,m^3/h$ and $82\,m^3/h$. So, operation at the flow $50\,m^3/h$ is very efficient and reasonable.

TABLE V
HEAD CHANGE AND THE TOT. HEAD AGAINST THE S.PRES. HEAD FOR MODEL AND FLOW

Flow (m^3/h)	Model	S. pres. head (10^{-1})	Vel. head (10^{-1})	Tot. head (10^{-1})	Tot. head / S. pres. head
18	(-2)	0.60	-0.76	-0.17	-0.28
	(-1)	0.46	-0.56	-0.11	-0.24
	Stand.	0.39	-0.44	-0.09	-0.23
	(1)	0.33	-0.38	-0.06	-0.18
	(2)	0.27	-0.32	-0.09	-0.33
50	(-2)	0.84	-1.41	-0.57	-0.68
	(-1)	0.81	-0.95	-0.14	-0.17
	Stand.	0.77	-0.93	-0.16	-0.21
	(1)	0.69	-0.79	-0.11	-0.16
	(2)	0.59	-0.65	-0.07	-0.12
82	(-2)	-0.32	-1.93	-2.35	6.34
	(-1)	-0.30	-1.22	-1.04	2.47
	Stand.	0.30	-1.20	-0.86	-2.87
	(1)	0.28	-0.82	-0.49	-1.75
	(2)	0.60	-0.73	-0.08	-0.13

IV. CONCLUSION

In this study, the effect of cross-sectional area on performance curve was investigated, and results were obtained as follows;

1. At low flow, backflow occurs along the circumferential direction regardless of model and this phenomenon is presented obviously near the tongue and vortex structure becomes symmetric with higher flow.
2. Static pressure head and velocity head intersect near section 3 in the circumferential direction. Static pressure head increases at low flow and velocity head increases at high flow, so they show opposite tendencies.
3. Total head in circumferential direction is almost uniform at low flow and the shape of curve becomes bent like an arrow with higher flow. Also the tendency of total head significantly departs from regular variation. Therefore a 10~30% smaller cross sectional area than the standard model is regarded as an available limited cross-sectional area and in the case of a smaller one than the limited cross-sectional area the possibility of surges occurring increases.
4. Based on the ratio in the discharge diffuser, Model (1) is that 10% larger than the standard model is optimum at low flow.

REFERENCES

[1] Sunsheng Yang, Fanyu Kong and Bin Chen"Research on pump volute design method using CFD," *International Journal of Rotating Machinery*, vol. 2011
[2] Weng Kong Chan, Yew Wah Wong and Wei Hu "Design considerations of volute geometry of a centrifugal blood pump" *Artificial Organs*
[3] Yew-Wah Wong, Weng-Kong Chan and Wei Hu "Effects of tongue *position* and base circle diameter on the performance of a centrifugal blood pump" *Artificial Organs*
[4] A.J.Stepanoff , *Centrifugal and Axial Flow Pumps*
[5] R.A. Van den Braembussche "Flow and loss mechanisms in volutes of centrifugal pumps"
[6] Kean Wee Cheah, Thong See Lee and Winoto S.H, "Numerical study of inlet and impeller flow structures in centrifugal pump at design and off-design points", *International Journal of Fluid Machinery and System*, vol.4, No. 1, January-March, 2011
[7] D. Hagelstein, K. Hillewaert, "Experimental and numerical investigation of the flow in a centrifugal compressor volute", *Transactions of the ASME*, vol 122, January 2000
[8] Kean Wee Cheah, Thong See Lee and Sonny H.Winoto "Unsteady analysis of impeller-volute interaction in centrifugal pump", *International Journal of Fluid Machinery and System*, vol.4, No. 3, July-September, 2011